Influence of water content on the ablation of skin with a 532 nm nanosecond Nd:YAG laser

Soogeun Kim
Tae Joong Eom
Sungho Jeong

Influence of water content on the ablation of skin with a 532 nm nanosecond Nd:YAG laser

Soogeun Kim,[a] Tae Joong Eom,[b,*] and Sungho Jeong[a,*]
[a]Gwangju Institute of Science and Technology, School of Mechatronics, 1 Oryong-dong Buk-gu, Gwangju 500-712, Republic of Korea
[b]Gwangju Institute of Science and Technology, Advanced Photonics Research Institute, 1 Oryong-dong Buk-gu, Gwangju 500-712, Republic of Korea

Abstract. This work reports that the ablation volume and rate of porcine skin changed significantly with the change of skin water content. Under the same laser irradiation conditions (532 nm Nd:YAG laser, pulse width = 11.5 ns, pulse energy = 1.54 J, beam radius = 0.54 mm), the ablation volume dropped by a factor of 4 as the skin water content decreased from 40 wt. % (native) to 19 wt. % with a change in the ablation rate below and above around 25 wt. %. Based on the ablation characteristics observed by *in situ* shadowgraph images and the calculated tissue temperatures, it is considered that an explosive rupture by rapid volumetric vaporization of water is responsible for the ablation of the high water content of skin, whereas thermal disintegration of directly irradiated surface layer is responsible for the low water content of skin. © *2015 Society of Photo-Optical Instrumentation Engineers (SPIE)* [DOI: 10.1117/1.JBO.20.1.018001]

1 Introduction

Nanosecond lasers are widely used for tissue ablation in various medical areas such as, ophthalmology,[1,2] dermatology,[3,4] and neurosurgery[5] due to the possibility of selectively removing target tissue with little collateral thermal damage.[6–8] During nanosecond laser ablation of a tissue, the results for tissue ablation are primarily governed by laser irradiation parameters such as laser energy density,[9,10] pulse width,[11,12] and wavelength[13,14] as reported in earlier studies. While the determination of optimum laser parameters for tissue ablation received the most attention in previous studies, the influence of water contained in a tissue target on ablation efficiency and/or mechanism was also of interest to researchers.[15–17] Since water undergoes a rapid vaporization and expansion during nanosecond laser irradiation, the ablation of a wet tissue can significantly be different from that of a dry tissue. In fact, the variation of ablation volume or rate due to the difference of water content was previously observed in laser tissue ablation. For example, from the study of XeCl excimer (308 nm) and Ho:YAG (2.1 μm) laser ablation of wet and dry dentin, Neev et al.[15] reported that the ablation rate of wet samples was nearly three times greater than that of dry samples at both wavelengths. In a similar study for the ablation of wet and dry dentin using two infrared lasers, Er:YAG laser (2.94 μm) and ErCr:YSGG laser (2.78 μm), Meister et al.[16] reported that a statistically significant enough influence of water content was observed only for the Er:YAG laser. For the soft tissue case, from the ablation of the collagen matrix of calf skin with an ArF excimer laser (193 nm), Tsunoda et al.[17] reported that the ablation threshold for a wet sample was lower than that of the dry sample, but the ablation rate of the wet sample was about five times greater than that of dry sample. Except for Tsunoda et al.'s work,[17] the authors could find no other study

about the effects of water content on soft tissue ablation. In addition, earlier research about the influence of water content on ablation characteristics was carried out mostly with ultraviolet or infrared lasers.

Recently, however, interest in the ablation of human skin using a Q-switched visible Nd:YAG laser (532 nm) is increasing. For instance, from the study of laser ablation of stratum corneum for the enhancement of transdermal delivery of hydrophilic drugs using three different wavelengths of nanosecond Nd:YAG lasers (355, 532, and 1064 nm), Gomez et al.[18] reported that the 532 nm Nd:YAG laser could be an appropriate choice because the danger of mutagenic effects of ultraviolet radiation or the influence of infrared radiation on collagen could be avoided with the visible wavelength. In a similar study about the delivery of 5-aminolevulinic acid using an Er:YAG laser and a visible Nd:YAG laser, the same authors also reported that the 532 nm Nd:YAG laser enabled a more precise control of the ablation process.[19] The treatment of a pigmented lesion is another area for which a 532 nm Nd:YAG laser has been widely applied.[20–23] Benign epidermal pigmented lesions could be safely and effectively treated using a 532 nm Nd:YAG laser with little side effects like textural change or scarring.[20] Also, the use of a 532 nm Nd:YAG laser in combination with a 1064 nm Nd:YAG laser was reported to be more effective in pigment clearance than using a 1064 nm Nd:YAG laser alone.[22]

Since the optical[24,25] and mechanical properties[26,27] of a tissue are known to be significantly influenced by water content, the results of skin ablation using a 532 nm Nd:YAG laser are also expected to change notably by tissue water content as observed in the ultraviolet and infrared laser cases. Furthermore, the water content of human skin is known to vary between individuals,[28,29] regionally over the body of a person,[30] or by the relative humidity of the environment.[31] Therefore, for controlled

*Address all correspondence to: Sungho Jeong, E-mail: shjeong@gist.ac.kr;
Tae Joong Eom, E-mail: eomtj@gist.ac.kr

ablation of skin using a 532 nm Nd:YAG laser and accurate application of the technique, it is necessary to understand how the ablation results are influenced by tissue water content change.

In this study, the effects of water content on the ablation of porcine skin using a 532 nm nanosecond Nd:YAG laser are investigated. The change of ablation phenomena of the skin sample due to water content change was experimentally investigated by taking shadowgraph images and measuring the volume of ablation craters with optical coherence tomography (OCT). The optical and mechanical properties of a porcine skin sample at varying water content conditions were also measured. Then the temperature rise of the tissue at varying water content conditions during laser irradiation was calculated using a mathematical model that considered the water content and temperature dependency of optical properties. The difference of ablation results and possible mechanisms with respect to tissue water content are discussed.

2 Materials and Methods

2.1 Sample Preparation

The porcine skin samples in experiments were obtained from a local abattoir immediately after postmortem. Abdominal skin of a porcine was used as a substitute for human skin due to their similarity in structural characteristics.[32,33] The obtained samples were put into a saline solution and stored in a refrigerator at 4°C to minimize dehydration and structural changes until the experiment. All experiments were performed at room temperature within 24 h of the collection of samples.

The initial water content of the samples was measured to be about 40 wt. % with a moisture analyzer (MB45, Ohaus Corp.). To investigate the effect of water content, the initial water content of the samples was reduced by blowing with a cold dryer. During the dehydration, there was little thermal damage on the sample due to the low blowing temperature (about 30°C). Considering that only water is vaporized during drying while the mass of the tissue component remain the same, the water content of a sample after drying, w_t (wt. %), was calculated by

$$w_t = 1 - (1 - w_{t0}) \frac{M_0}{M}, \qquad (1)$$

where w_{t0} is the initial water content (wt.%), M_0 is the initial mass (g), and M is the mass (g) after drying of the sample.

2.2 Measurement of Optical and Mechanical Properties

The optical properties (absorption coefficient and reduced scattering coefficient) of porcine skin at 532 nm wavelength were estimated using an inverse adding-doubling program from the total reflectance and transmittance of porcine skin samples (thickness ≈ 500 μm) measured with a double-integrating sphere (AvaSphere-30, Avantes).[34,35] The measurements of total reflectance and transmittance were made over the water content range of 19wt. % to 40 wt. % for every 3 wt. % with five samples at each water content condition. Since the temperature of a tissue irradiated by a nanosecond laser can rise well above the surrounding temperature, up to the level causing thermal damage of the tissue, the optical properties of thermally damaged tissue were also estimated using the same procedure. For the preparation of thermally damaged porcine skin, both sides of the

samples were briefly in contact with a heated aluminum plate (100, 200, or 300°C) and detached.

The variation of ultimate tensile strength (UTS) of the porcine skin sample with respect to water content was also measured using a 30 kN electro-mechanical testing machine (Instron 5567, Instron). The test was conducted by placing an hourglass-shaped sample (thickness ≈ 1 mm) between the upper and lower grips of the machine and loading in tension (tension speed = 20 mm/ min). By using the load-extension curve obtained from tension test with the original cross-sectional area of the test sample, the UTS of each sample was calculated. Test results revealed that the UTS of native porcine skin samples could be measured with high reproducibility. However, the measured UTS values of lower water content samples showed large fluctuations, preventing us from finding a clear tendency with respect to water content. Thus, to obtain a clear UTS curve with respect to the water content, the UTS measurement was carried out at three widely different water content conditions, namely, at a well dried state (5.3 wt. %), at one low water content condition (19 wt. %), and with the native porcine skin sample (40 wt. %). The 5.3 wt. % sample was prepared by air-drying at room temperature for about 12 h. For each water content condition, the UTS measurement was repeated five times. Note that the UTS measurement of the thermally damaged samples was not attempted due to the poor reproducibility observed in the undamaged low water content samples.

2.3 Skin Ablation

A Q-switched 532 nm Nd:YAG laser (Powerlite DLS Plus, Continuum) was used for the ablation of porcine skin samples. The laser beam had a spatially flat top and temporally Gaussian profiles and the pulse width at $1/e$ of its maximum intensity (τ) was 11.5 ns. The laser pulse energy (E_0) and beam radius (w_0) on the sample surface were 1.54 J and 0.54 mm (laser energy density = 168.11 J/cm^2), respectively.

The ablation of porcine skin samples (thickness ≈ 1 mm) was conducted under normal atmospheric conditions for water content values in the same as in the optical property measurement (19, 22, 25, 28, 31, 34, 37, and 40 wt. %). To examine the change of crater volume with respect to pulse number, each spot on the sample was irradiated with a different number of laser shots (1, 3, 5, 10, and 15), and the same experiment was repeated three times for all laser shot conditions. The volume of ablation craters produced on the porcine skin samples of different water content with different numbers of laser shots were immediately measured after laser ablation using a house-developed Fourier domain OCT (FD-OCT) system. The FD-OCT was equipped with a high speed wavelength-swept laser (SSOCT-1310, Axsun; center wave length = 1.31 μm) that was coupled into the source arm of a fiber-based OCT interferometer. The interference signals between the ablated sample and the reference mirror of the FD-OCT were acquired using a high speed digitizer (PX14400, Signatec Inc.) and processed using a parallel computing technique to produce a real-time image. Each porcine skin sample was scanned with the FD-OCT over the volume of 5 mm(x) × 5 mm(y) area on the surface times 4.5 mm (z) along the depth; specifically, a cross-sectional OCT image in the x-z plane was repeatedly taken every 10 μm along the y direction. For the estimation of crater volume, the pixel numbers within a crater were counted from these images.
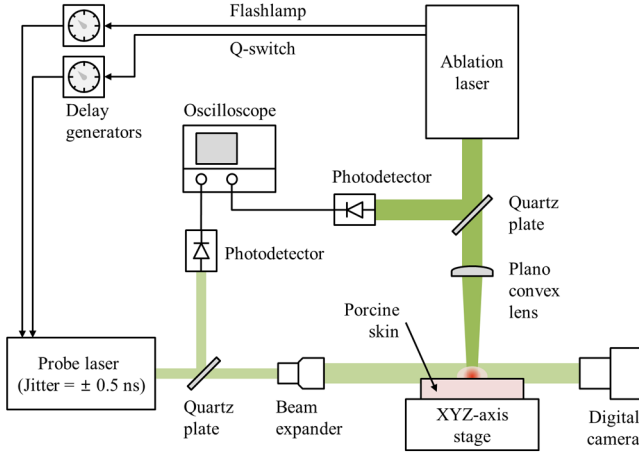
Fig. 1 Schematic of the experimental setup for laser ablation of porcine skin and shadowgraph imaging. The delays of flashlamp and Q-switch of the probe laser were controlled separately to enhance timing accuracy.

2.4 Shadowgraph

To examine the possible changes in the ablation mechanism with respect to water content, the ablation of tissue at different water content conditions was imaged *in situ* at varying delay time from the moment of laser irradiation using the shadowgraphy technique.[36] The shadowgraphy setup adopted another Q-switched 532 nm Nd:YAG laser (Minilite I, Continuum, $\tau = 5$ ns, jitter with external trigger $= \pm 0.5$ ns) as the probe beam as shown in Fig. 1 and the image was captured on a digital camera (D-100, Nikon). For precise adjustment of the delay time between the ablation laser pulse and the probe laser pulse, the flashlamp and Q-switch of the probe laser were externally triggered using the sync output signals of the flashlamp and the Q-switch of the ablation laser, respectively, using two delay generators (DG535 and DG645, Stanford Research Systems Inc.). The actual delay time was then measured using two photodetectors (DET36A/M, Thorlabs Inc.) by collecting partially reflected laser beams from the quartz plates placed in the paths of the two laser beams. Using this setup, the images of the expanding shock wave and ablated particles were captured over a wide range of delay times, from about 150 ns to tens of μs.

2.5 Calculation of Tissue Temperature

The irradiation of tissue by an intense laser results in a rapid rise of tissue temperature well above the surrounding temperature. The level of tissue temperature reached by laser irradiation and its temporal and spatial profiles are closely related to the tissue removal process, and can provide valuable information about the ablation mechanism. The temperature rise of tissue under laser irradiation can be described by the bioheat transfer equation as[37]

$$\rho c \frac{\partial T(r, z, t)}{\partial t} = k \nabla^2 T(r, z, t) + Q_p + Q_s, \tag{2}$$

where $T(r, z, t)$, ρ, c, and k are the temperature (°C), density (kg/m³), specific heat (J/kg°C), and the thermal conductivity (W/m°C) of tissue, respectively, and Q_s is the heat generation (W/m³) due to laser light absorption. Q_p represents the heat transfer (W/m³) caused by blood perfusion, which, however,

was ignored in this study because of the absence of blood perfusion in the *in vitro* porcine skin samples. The first term on the right-hand side of Eq. (2) is a thermal conduction term. The thermal diffusion length of porcine skin ($= 2\sqrt{\alpha\tau}$ with $\alpha \approx 1 \times 10^{-7}$ m²/s) during laser irradiation is only on the order of tens of nm, whereas the optical penetration depth of the 532 nm laser light is at least several hundreds of μm. Thus, for a nanosecond laser, thermal conduction through the sample during laser irradiation can be ignored. Then, Eq. (2) is simplified to

$$\rho c \frac{\partial T(r, z, t)}{\partial t} = Q_s, \tag{3}$$

and the solution of Eq. (3) becomes

$$T(r, z, t) = T_0(r, z, t) + \int_0^{t_p} \frac{Q_s}{\rho c} dt, \tag{4}$$

where $T_0(r, z, t)$ is the initial temperature (°C) of tissue, and t_p is the entire duration (s) of laser light emission. For strongly scattering tissue, the heat generation term, Q_s, can be expressed by[38]

$$Q_s = \mu_a [\Phi_d(r, z, t) + \Phi_{ri}(r, z, t)], \tag{5}$$

where μ_a is the absorption coefficient (m⁻¹) of tissue, and $\Phi_d(r, z, t)$ and $\Phi_{ri}(r, z, t)$ are the diffuse fluence rate (W/m²) and reduced incident fluence rate (W/m²), respectively. Under the conditions of cylindrical symmetry and a normally incident laser beam, the diffuse fluence rate can be obtained by solving the following diffusion equation [39,40]

$$\frac{1}{\nu} \frac{\partial \Phi_d(r, z, t)}{\partial t} = D \nabla^2 \Phi_d(r, z, t) - \mu_a \Phi_d(r, z, t) + (3D\mu_t g + 1)\mu_s \Phi_{ri}(r, z, t), \tag{6}$$

where ν is the speed of light (m/s) in tissue, g is the anisotropy factor, μ_s is the scattering coefficient (m⁻¹), and $\mu_t = \mu_a + \mu_s$ is the attenuation coefficient (m⁻¹) of tissue. The diffusion coefficient, D (m), is represented by

$$D = \frac{1}{3(\mu_a + \mu_s')}, \tag{7}$$

where $\mu_s' \equiv \mu_s(1 - g)$ is the reduced scattering coefficient (m⁻¹). For a laser beam with a spatially flat top and temporally Gaussian profiles, the reduced incident fluence rate is expressed by

$$\Phi_{ri}(r, z, t) = (1 - R) \frac{2E_0}{\pi^{1.5} w_0^2 \tau} \exp\left[-\frac{(t - t_0)^2}{(\tau/2)^2}\right] \exp(-\mu_t z), \tag{8}$$

where R is the reflectance at normal incidence, E_0 and w_0 are the laser pulse energy (J) and beam radius (m) at the sample surface, respectively, and t_0 (s) is when the maximum intensity occurs.

3 Results and Discussions

3.1 Optical and Mechanical Properties

Figure 2 shows the measured absorption (μ_a) and reduced scattering (μ_s') coefficients of the porcine skin samples at different
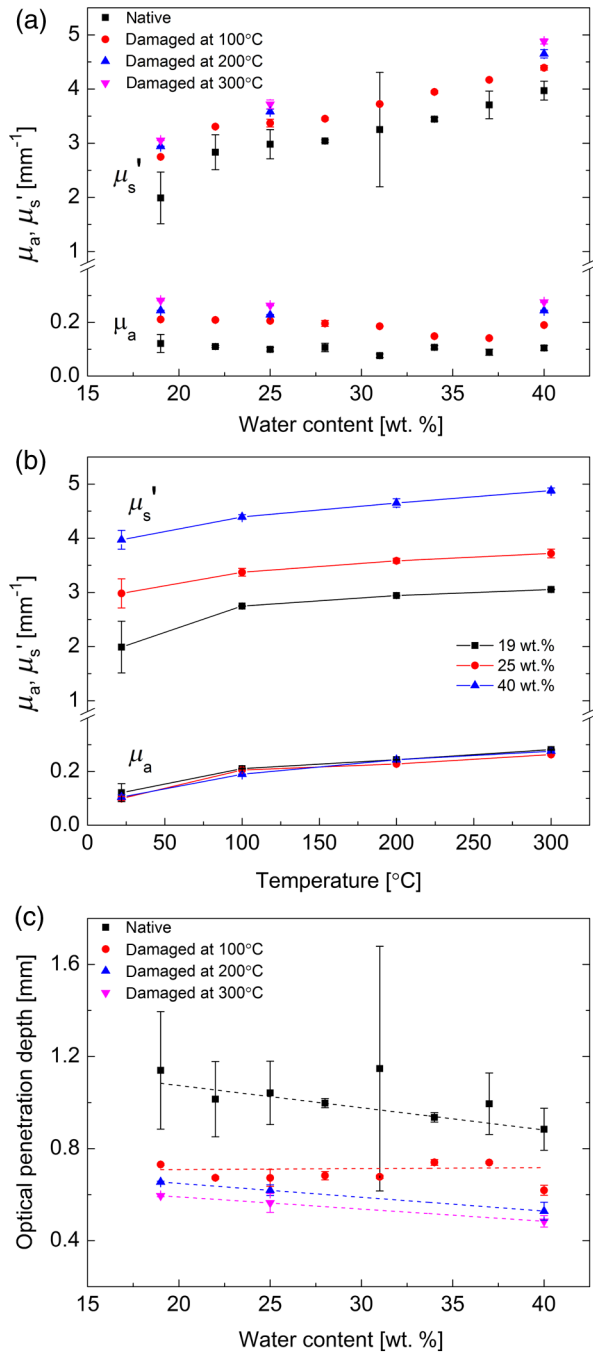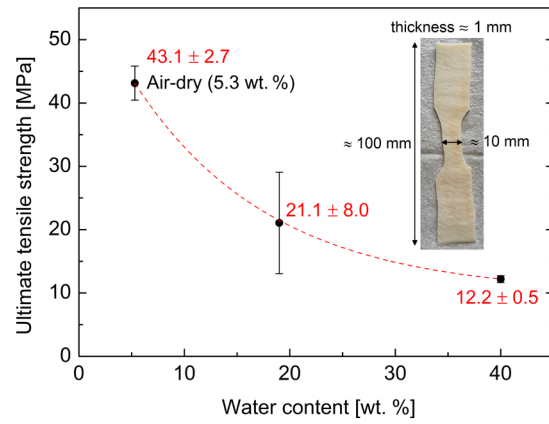
Fig. 3 Ultimate tensile strength of native porcine skin at varying water content.

components by the shrinkage of the thermally damaged sample.[8,41] On the other hand, μ_s' showed a clear increase for both increasing water content and increasing damage temperature. The observed increase of μ_s' at an increased water content may be attributed to the refractive index mismatch between collagen fibrils and interstitial space as a result of the increased water within the interstitial space[24] while that for the increased damage temperature may be attributed to the change in size and/or number of scattering particles in thermally denatured tissue.[42]

From the measured absorption and reduced scattering coefficients, the optical penetration depth of native or thermally damaged porcine skin at different water content can be estimated by[39]

$$\delta = \frac{1}{\sqrt{3\mu_a(\mu_a + \mu_s')}}. \tag{9}$$

The results for optical penetration depth calculation in Fig. 2(c) show that the optical penetration depth is generally inversely proportional to tissue water content. These results reveal that the optical penetration depth of 532 nm wavelength light in skin decreases as the skin water content increases or when the tissue is thermally damaged.

Figure 3 shows the measured UTS of native porcine skin samples of 5.3 (air-dry), 19, and 40 wt. % water content with the photograph of an actual test sample. These data show that the UTS of the porcine skin sample increases rapidly as the water content decreases. Previously, it was reported that the strength of a collagen-rich tissue like skin increased with dehydration due to the increase of the density of cross-link in collagen fibrils.[26,27] Since the porcine skin used in the present study mostly consisted of collagen, the observed increase of UTS with dehydration may also be attributed to the density change of the cross-link in collagen fibrils. The observed change of UTS with respect to water content is understood to be closely related to the laser ablation behavior of the porcine skin sample to be discussed below.

3.2 Ablation Craters

Figure 4 shows the three-dimensional (3-D) OCT images of ablation craters produced on porcine skin samples of different water content for varying numbers of laser shots. On the 3-shot images, it is seen that tissue around the crater rim of the 19 wt. % sample underwent clearer change, possibly revealing the result
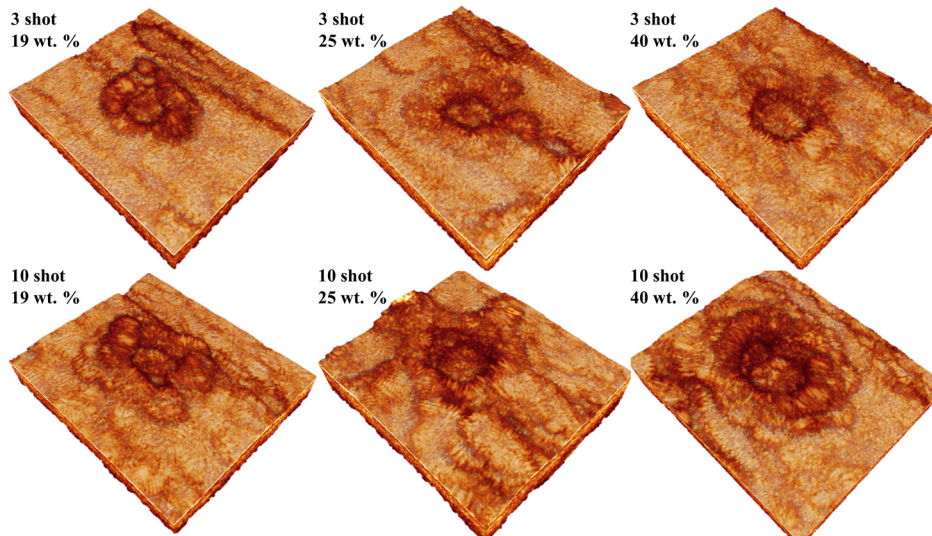

Fig. 2 Variation of the measured absorption (μ_a) and reduced scattering (μ_s') coefficients of porcine skin with respect to (a) water content and (b) damage temperature, (c) the optical penetration depth calculated from these coefficients.

water content and temperatures. The μ_a and μ_s' values of the native sample and the sample thermally damaged at 100°C were measured for all water content conditions, whereas those of the samples thermally damaged at 200°C and 300°C were measured only for the 19, 25, and 40 wt. % to check the overall trends. First, Fig. 2(a) shows that μ_a was not much influenced by the change of tissue water content. However, when damaged at 100°C, μ_a almost doubled from the value of the native tissue and kept increasing as shown in Fig. 2(b). Although the reason for the μ_a increase of the thermally damaged sample is not immediately obvious, one possible explanation is the denser packing of tissue

Fig. 4 Three dimensional optical coherence tomography (OCT) images of the porcine skin samples of different water content irradiated by multiple laser shots.

of stronger tissue thermal damage, than the 25 and 40 wt. % samples. After 10 shots, all the samples basically showed the same morphology around the crater. These images also show that the crater diameter produced by the same number of shots slightly increased with water content.

For quantitative analysis of the crater shape and volume, cross-sectional OCT images of the laser ablation craters were taken as shown in Fig. 5. For the estimation of crater width and depth, an ablation crater was defined by the removed tissue volume below the original sample surface (indicated by a dashed line on the 3-shot images of 19 and 40 wt. % samples). Although the elevation of material above the original sample surface around the crater rim is observed in the cross-sectional OCT images, especially for the 19 wt. % sample, the crater volume
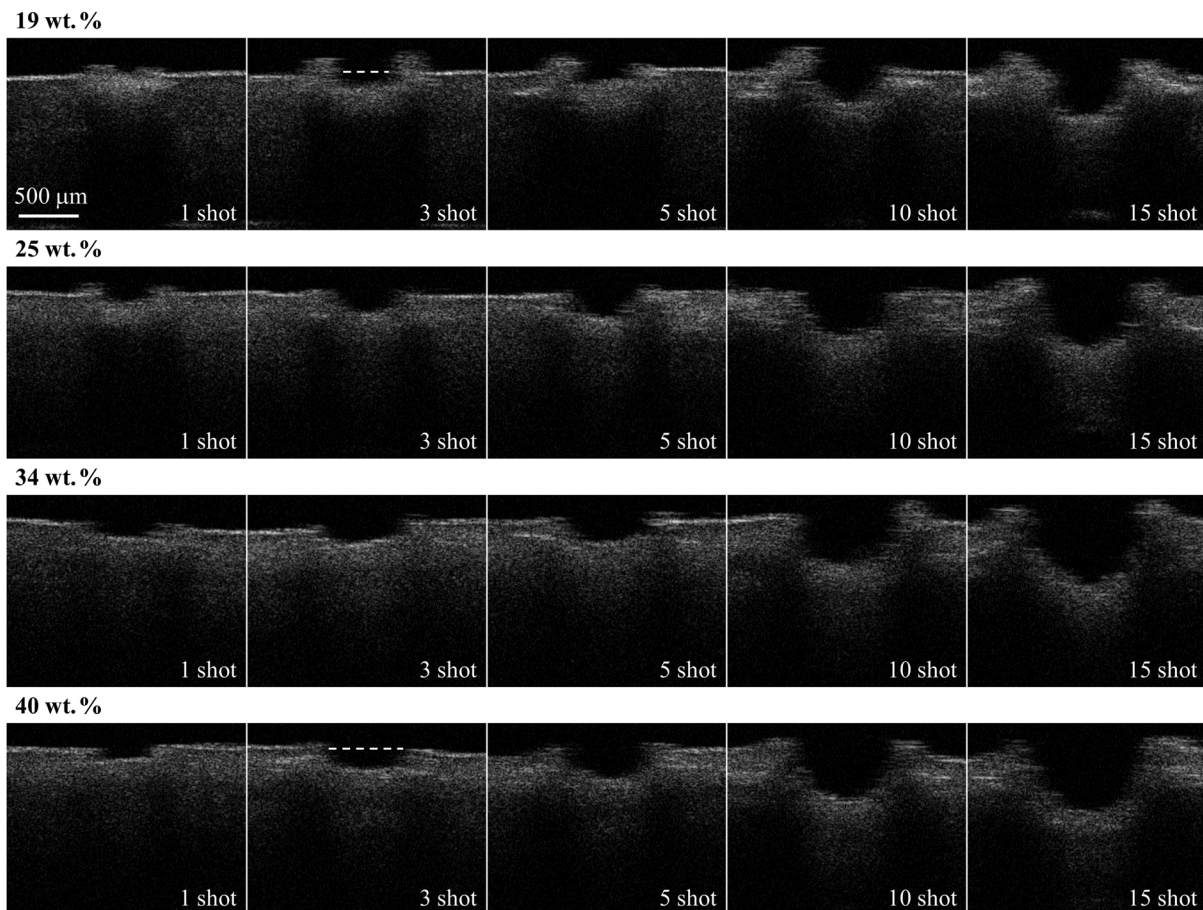

Fig. 5 Cross-sectional OCT images of the porcine skin samples for varying laser shots.

of these samples was still defined by the volume underneath the original sample surface. Using the original sample surface as the reference, the ablation width, depth, and volume of the craters were measured by counting pixels from the OCT images. The pixel sizes on a cross-sectional image along the x (lateral) and z (depthwise) directions were 5 and 6.43 μm, respectively. The crater volume was then estimated by adding the areas measured from multiple cross-sectional images taken along the y direction with 10-μm interval.

Figure 6 shows the variation of maximum width, maximum depth, and total volume of ablation craters obtained from the OCT images with respect to tissue water content for different numbers of laser shots. For samples with water content below 25 wt. %, the tissue was weakly ablated by a single pulse as observed by the small crater width and depth in Figs. 6(a) and 6(b). For multipulse ablation, the ablation width continuously increased with tissue water content, which is consistent with the change of crater size observed from the 3-D images in Fig. 4. On the other hand, the ablation depth showed a rather rapid increase with water content up to about 25 wt. % above which, however, it remained nearly the same. Note that the optical penetration depth of porcine skin over this water content range decreased almost linearly, Fig. 2(c). The similarity in measured crater depths for samples with 25 wt. % or higher water content is thus understood to imply that optical penetration depth is not the governing factor for the ablation of skin samples over 25 wt. % water content. The combined effect of ablation width and depth change is represented by the ablation volume in Fig. 6(c) which reveals a rather rapid increase of ablation volume up to around 25 wt. % followed by a slower but consistent increase. The actual ablation volume increase for the 3-, 5-, or 10-shot craters was about 2.1–2.7 times as the water content increased from 19 wt. % to 25 wt. % and about 1.4–2.3 times for the water content increase from 25 wt. % to 40 wt. %. Since the laser parameters were kept the same during the ablation of these craters, the observed differences in ablation depth and volume with respect to skin water content are understood to suggest that there exists a fundamental difference in ablation processes between the high and low water content skin samples, especially below and above around 25 wt. %.

3.3 Mechanism of Tissue Removal

To examine the difference in ablation processes between high and low water content skin samples, *in situ* images of the ablation target were taken at various elapsed times from the moment of laser irradiation. Figure 7 shows the shadowgraph images of tissue material being ablated from the porcine skin samples of 19, 25, and 40 wt. % water content. Note that the image at a given delay time for each water content condition was taken independently from the images of other delay times; that is, each shadowgraph image was taken by irradiating a single laser shot on a new spot on the same porcine skin after setting a new delay time. The shadowgraph images in Fig. 7 show that there exists a distinct difference in tissue removal phenomena between the low (19 wt. %) and high (40 wt. %) water content porcine skin samples. First, the amount of tissue eventually removed from the sample appears significantly greater in the case of the 40 wt. % sample than the 19 wt. % one, which is clear from the images at 448, 948, and 2048 ns delay times of these water content samples. This observation is consistent with the increase of ablation volume at the higher water content in Fig. 6(c). Next, for the 40 wt. % sample, a significant portion
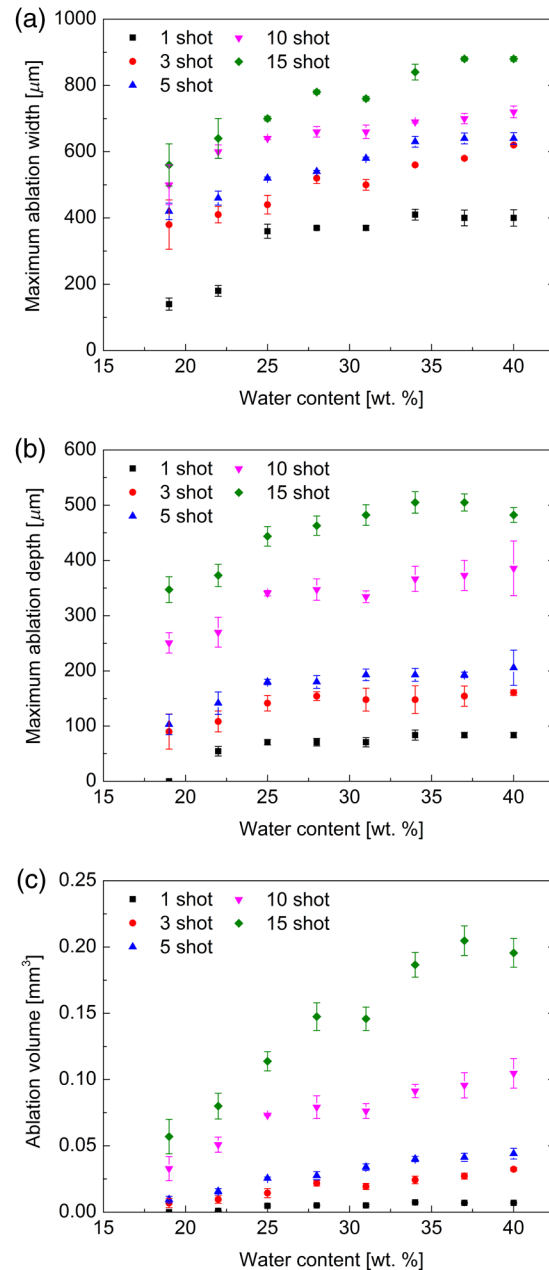

Fig. 6 Variation of (a) maximum ablation width, (b) maximum ablation depth, (c) ablation volume with respect to tissue water content for different numbers of laser shots.

of the ablated tissue appears to be interlaced and stretched, and the ablation mass included relatively large pieces of tissue fragments (see the image for 2048 ns delay). On the other hand, the tissue removed from the 19 wt. % sample appears to consist of relatively much finer independent tissue fragments (also see the image for 2048 ns delay).

The shadowgraph images also provide qualitative information about the momentum of ablated tissue material. The expansion of ablated tissue material for the 40 wt. % sample appears to have maintained a strong momentum until 2048 ns after the ablation laser pulse. On the contrary, the expansion of the 19 wt. % sample seems to have maintained a momentum similar to that of the 25 or 40 wt. % samples during the early time, but started losing momentum as early as 448 ns with an accompanied decrease of ablation mass. The momentum change of the
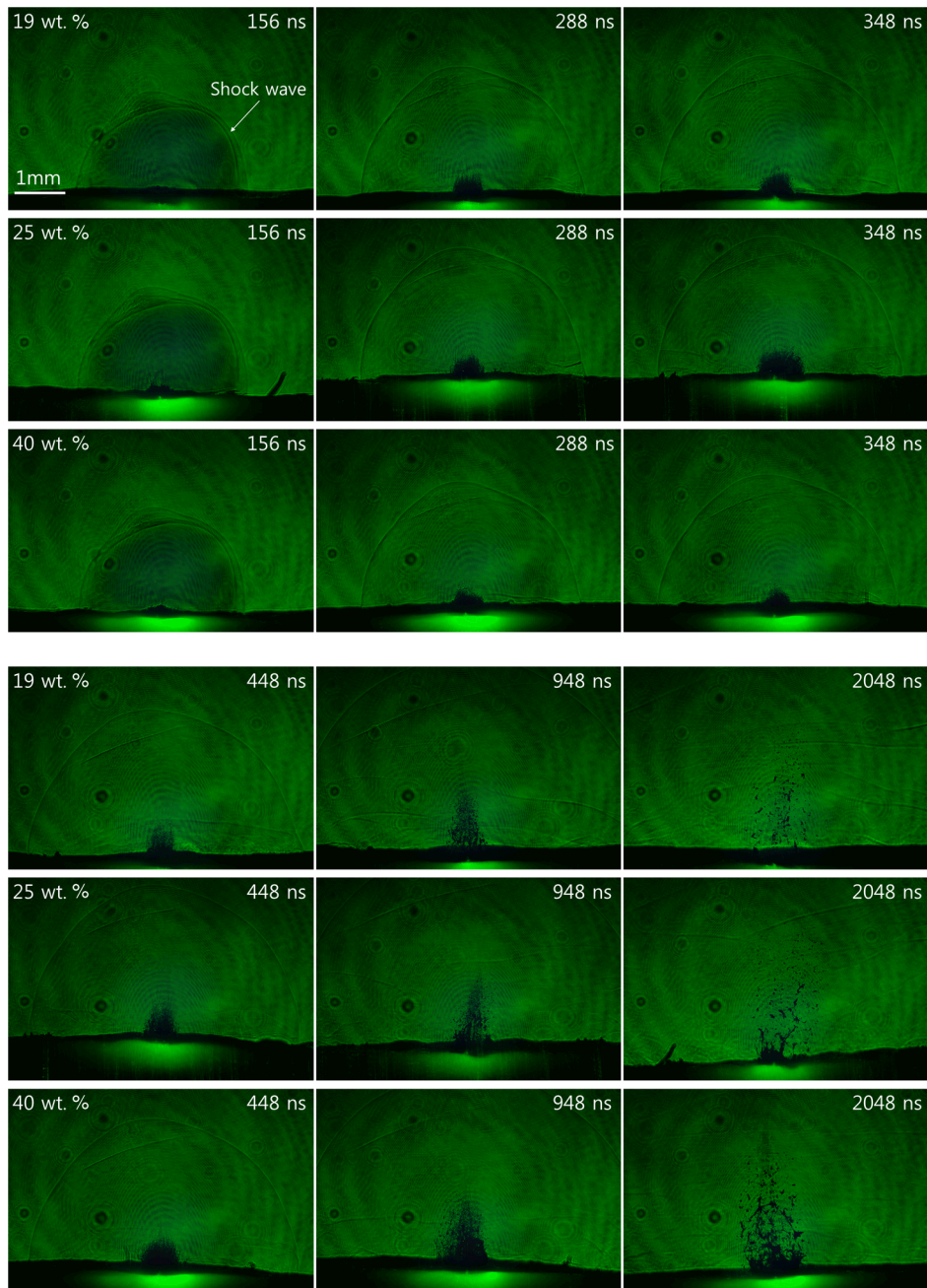
Fig. 7 Shadowgraph images of the porcine skin samples of different water content at varying delay times.

ablated mass can be more clearly observed from the shock wave velocity. Figure 8 shows the position of the shock wave front from the sample surface with respect to the delay time. The initial shock wave velocity (slope) of the 19 wt. % sample is greater than that of the 40 wt. % one which, however, clearly dropped below that of the 40 wt. % sample after around 400 ns. The reduced shock wave velocity is possibly because the ablation of the 19 wt. % sample was quickly weakened as the laser irradiation ceased. On the other hand, the shock wave velocity of the 40 wt. % sample was hardly retarded with time, which is understood to imply that the ablation of the 40 wt. % sample continued over this period, independently from the cessation of the laser irradiation. These changes in shock wave velocity of the 19 and 40 wt. % samples are consistent with the trend in

ablation mass changes at around 400 ns that is observed in the shadowgraphs in Fig. 7.

The observed differences in ablation volume and momentum between the low and high water content samples are likely to reflect the difference in ablation mechanisms between these two samples. Since the laser ablation of tissue is closely related to the temperature level induced in the sample and to the mechanical property of tissue, the spatial and temporal changes of the tissue temperature were calculated using the bioheat transfer equation, Eq. (4), for three water content conditions (19, 25, and 40 wt. %). For the calculation of diffuse fluence rate, $\Phi_d(r, z, t)$, in the heat generation term, the diffusion equation, Eq. (6), was solved at each time step with the consideration of water content and temperature dependency of μ_a and μ_s' shown
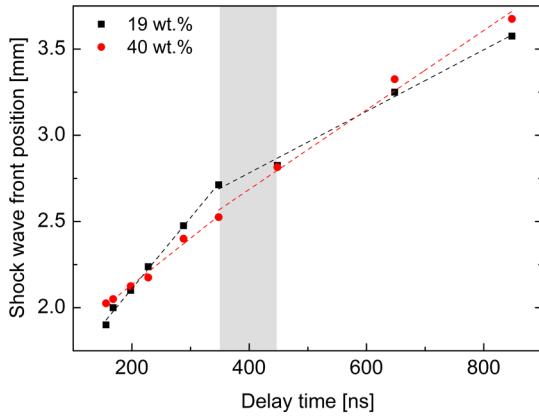
Fig. 8 Shock wave front position of the low and high water content samples with respect to delay time.
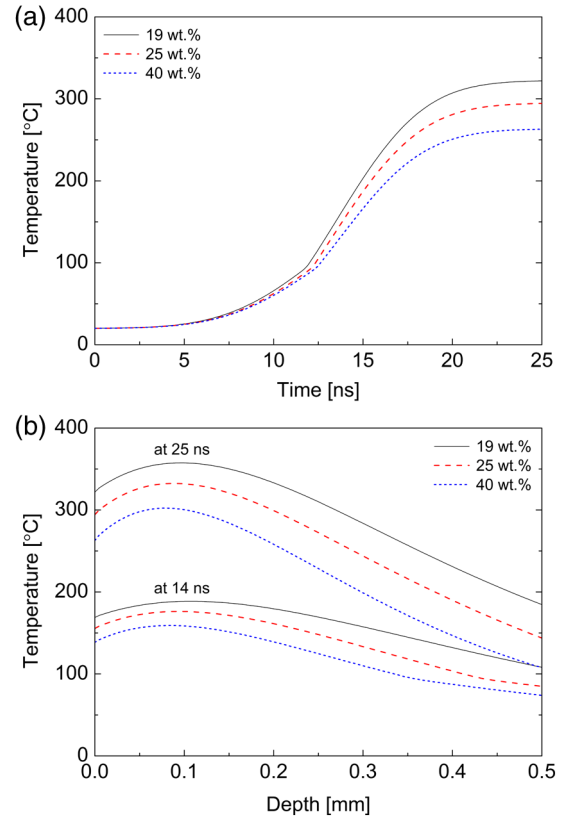

Fig. 9 (a) Temporal change of tissue surface temperature and (b) depthwise temperature distribution of the porcine skin samples with different water content during laser irradiation.

in Fig. 2. Since the volume of porcine skin sample used in the experiments (about 0.4 cm^3 = 2 cm × 2 cm × 0.1 cm) showed little change with water content (<3%), the density of tissue decreased as the tissue water content was reduced. The density of each water content sample was calculated by measuring the sample mass with an electronic balance (XB 220A, Precisa) to be 874 ± 57, 944 ± 70, and 1180 ± 77 kg/m^3 (average and standard deviation of ten sample measurements) for the 19, 25, and 40 wt. % samples, respectively. The specific heat of the porcine skin sample at varying water content conditions was calculated by the following equation:[43]

$$c = 4200 w_t + 1090 w_p + 2300 w_f, \qquad (10)$$

where w_p and w_f are the mass fraction of proteins like collagen and fat, respectively. Since the porcine skin used in this study mostly consisted of water (initially about 40 wt. %) and collagen (initially about 60 wt. %), the third term on the right-hand side of Eq. (10) was ignored. Then, the specific heat of the 19, 25, and 40 wt. % samples was calculated to be 1452, 1704, and 2334 J/kg · °C, respectively, for a constant w_p of 0.6. Other values used for the calculation include $T_0 = 20°C$, $g = 0.86$,[44] $R = 0.023$,[45] $E_0 = 1.54$ J, $w_0 = 0.54$ mm, $\tau = 11.5$ ns, and $t_0 = 12.5$ ns.

Figure 9 shows the results of tissue temperature calculations for different water content values. The surface temperature of all samples continuously increased during the laser irradiation ($t_p = 25$ ns) as shown in Fig. 9(a). Among the three samples, the temperature of the 19 wt. % sample was highest because of the relatively lower density and specific heat of the low water content sample. Figure 9(b) shows the distribution of temperature along the depth (surface is at the origin) at the moment of laser turn off; the profiles at an intermediate time (14 ns) are also shown to check the transient development of the temperature profiles. Note that the maximum tissue temperature ($T_{\max}$) took place below the sample surface, which was known to occur in a tissue satisfying $\mu_s' \gg \mu_a$ because heat generation in this case becomes maximum below the surface due to backscattering.[46] The predicted $T_{\max}$ and its depth were (357°C, 95 μm), (332°C, 90 μm), and (302°C, 80 μm) for the 19, 25, and 40 wt. % samples, respectively.

Theoretically, superheating of water can continue until it reaches the spinodal limit which is equal to about $0.8T_c$ at atmospheric pressure where T_c is the critical temperature of water (374.14°C).[8] If the water is heated beyond the spinodal

limit, stability will be lost and an irreversible vaporization takes place. A similar vaporization may have been possible for the water within heated tissue when the tissue temperature rose beyond the spinodal limit. Once initiated, the vaporization would be likely to occur collectively and nearly simultaneously over the irradiated volume, and the rapid increase of vapor volume may result in an explosive rupture of tissue if the pressure buildup exceeded the UTS of tissue.[8] The saturation pressure of water, $P_{\text{sat}}(T_l)$ (Pa), at the spinodal temperature (about 300°C) can be estimated with the Clausius-Clapeyron equation[47]

$$P_{\text{sat}}(T_l) = P_{\text{atm}} \exp\left[\frac{M_w h_{lv}}{R_{\text{gas}}}\left(\frac{1}{T_{\text{atm}}} - \frac{1}{T_l}\right)\right], \qquad (11)$$

where T_l is the water temperature (K), P_{atm} is the atmospheric pressure (Pa), M_w is the molecular weight of water (0.018 kg/mol), h_{lv} is the latent heat of vaporization of water at T_{atm} (2.26 × 10^6 J/kg), R_{gas} is the gas constant (8.314 J/K · mol), and T_{atm} is the boiling temperature (373.12 K) of water at P_{atm}. Using Eq. (11), the saturation pressure of water at the spinodal temperature was calculated to be about 9.8 MPa.

Note that the measured UTS of native porcine skin at 40 wt. % water content in Fig. 3 was 12.2 ± 0.5 MPa, greater than the saturation pressure at the spinodal temperature of water. However, it is known that laser heating causes thermal denaturation of tissue for which the degree of denaturation depends on the temperature level and exposure time. In general, the higher the tissue temperature is, the shorter the exposure time for denaturation. For the case of collagen-rich tissue like skin, it was reported that tissue became thermally denatured when exposed

to 125°C over 1 ns.[48] It was also known that tissue denaturation was accompanied by the destruction of intermolecular hydrogen bonds,[48] which would result in the weakening of the mechanical integrity of tissue. The results for tissue temperature calculation in Fig. 9(a) showed that tissue temperature and exposure time are well beyond the denaturation criteria reported in the previous study.[48] Therefore, it is likely that the porcine skin samples irradiated by the 532 nm nanosecond Nd:YAG laser in this study were denatured to the state at which their UTS values became lower than those at native conditions in Fig. 3. For the 40 wt. % sample, the UTS of native sample (12.2 ± 0.5 MPa) is only about 25% higher than the saturation pressure of water at spinodal temperature. If the decrease of UTS due to denaturation had exceeded this difference, which is considered to be possible, a volumetric and explosive rupture of weakened tissue could have taken place as a result of the rapid expansion of water vapor at the spinodal temperature. The ablation pattern of the 40 wt. % sample in the shadowgraph (2048 ns delay in Fig. 7) characterized by the interlaced and stretched tissue material, large tissue fragments, and splash-like tissue shape at the sample surface is considered to be highly suggestive of an explosive rupture of thermally damaged tissue. In this case, the ablation depth will be determined by the maximum tissue temperature. It is seen in Fig. 9(b) that the maximum tissue temperature took place nearly at the same depth for the 25 and 40 wt. % samples, which may be why the measured ablation depth in Fig. 6(b) was almost the same for samples with water content between 25 and 40 wt. %.

On the other hand, the shadowgraphs of 19 wt. % sample lack the above described characteristics of an explosive rupture. Although the calculated maximum tissue temperature of the 19 wt. % sample (357°C) is even higher than that of the 40 wt. % sample (302°C), the average UTS of the native 19 wt. % sample (21.1 MPa) was over twice that of the saturation pressure of water at the spinodal temperature (9.8 MPa). Because of this high initial UTS, the UTS of the thermally denatured 19 wt. % sample could have been still greater than the saturation pressure of water. Furthermore, the amount of water that could contribute to the pressure buildup upon reaching of the spinodal temperature was less than half of the 40 wt. % case. Based on these considerations, it is postulated that vapor pressure buildup inside the 19 wt. % sample was insufficient to overcome the strength of tissue in spite of weakening due to thermal damage. Instead, it is assumed that the observed tissue ablation resulted mainly from disintegration of thermally denatured tissue at the sample surface. The relatively homogeneous shape and size of ablation particles observed in the shadowgraphs of 19 wt. % sample in Fig. 7 (see images for the 948 ns and 2048 ns delay) with a few large fragments are supportive of this assumption. In the case of surface ablation, the ablation mass starts diminishing immediately after the laser turns off. The initially strong but rapidly falling momentum of the 19 wt. % sample observed from the shock wave velocity (Fig. 8) is understood as another supporting evidence of surface ablation.

4 Conclusion

This study demonstrated that the ablation characteristics of skin by a 532 nm nanosecond Nd:YAG laser change significantly with skin water content. Compared with the native skin (40 wt. %), the ablation volume of a dried skin (19 wt. %) dropped nearly by a factor of 4 under the same laser irradiation conditions. The experimental and numerical results were highly suggestive that an explosive rupture by volumetric vaporization of water occurred during the ablation of high water content skin, whereas surface ablation of the thermally denatured tissue was dominant for low water content skin. Since a 532 nm nanosecond Nd:YAG laser is increasingly adopted in laser therapy while skin water content is known to vary between individuals and/or bodily regions, it is considered that the observed water content dependency of skin ablation should be considered for controlled tissue ablation using a 532 nm nanosecond Nd:YAG laser.

References

1. J. M. Krauss, C. A. Puliafito, and R. F. Steinert, "Laser interactions with the cornea," *Surv. Ophthalmol.* **31**(1), 37–53 (1986).
2. L. M. Shanyfelt et al., "Effects of laser repetition rate on corneal tissue ablation for 193-nm excimer laser light," *Lasers Surg. Med.* **40**(7), 483–493 (2008).
3. R. R. Anderson et al., "Selective photothermolysis of cutaneous pigmentation by Q-switched Nd:YAG laser pulses at 1064, 532, and 355 nm," *J. Invest. Dermatol.* **93**(1), 28–32 (1989).
4. E. L. Tanzi, J. R. Lupton, and T. S. Alster, "Lasers in dermatology: four decades of progress," *J. Am. Acad. Dermatol.* **49**(1), 1–34 (2003).
5. M. H. Niemz, *Laser-Tissue Interactions: Fundamentals and Applications*, 3rd enlarged ed., Springer, Berlin (2007).
6. R. R. Anderson and J. A. Parrish, "Selective photothermolysis: precise microsurgery by selective ablation of pulsed radiation," *Science* **220**(4596), 524–527 (1983).
7. J. Boulnois, "Photophysical processes in recent medical laser developments: a review," *Lasers Med. Sci.* **1**(1), 47–66 (1986).
8. A. Vogel and V. Venugopalan, "Mechanisms of pulsed laser ablation of biological tissues," *Chem. Rev.* **103**(2), 577–644 (2003).
9. H. W. Kang, J. Kim, and Y. S. Peng, "In vitro investigation of wavelength-dependent tissue ablation: laser prostatectomy between 532 nm and 2.01 μm," *Lasers Surg. Med.* **42**(3), 237–244 (2010).
10. T. Kita et al., "In vitro study on selective removal of bovine demineralized dentin using nanosecond pulsed laser at wavelengths around 5.8 μm for realizing less invasive treatment of dental caries," *Lasers Med. Sci.* (2014).
11. D. Fried et al., "Mechanism of water augmentation during IR laser ablation of dental enamel," *Lasers Surg. Med.* **31**(3), 186–193 (2002).
12. M. Ivanenko et al., "Ablation of hard bone tissue with pulsed CO2 lasers," *Med. Laser Appl.* **20**(1), 13–23 (2005).
13. S. Sato et al., "Nanosecond, high-intensity pulsed laser ablation of myocardium tissue at the ultraviolet, visible, and near-infrared wavelengths: in-vitro study," *Lasers Surg. Med.* **29**(5), 464–473 (2001).
14. X. Hu et al., "Mechanism study of porcine skin ablation by nanosecond laser pulses at 1064, 532, 266, and 213 nm," *IEEE J. Quantum Electron.* **37**(3), 322–328 (2001).
15. J. Neev et al., "The effect of water content on UV and IR hard tissue ablation," *Proc. SPIE* **2323**, 292–299 (1995).
16. J. Meister et al., "Influence of the water content in dental enamel and dentin on ablation with erbium YAG and erbium YSGG lasers," *J. Biomed. Opt.* **11**(3), 034030 (2006).
17. K. Tsunoda et al., "Characterization of water contribution to excimer laser ablation of collagen," *J. Photochem. Photobiol. A-Chem* **145**(3), 195–200 (2001).
18. C. Gomez et al., "Laser treatments on skin enhancing and controlling transdermal delivery of 5-fluorouracil," *Lasers Surg. Med.* **40**(1), 6–12 (2008).
19. C. Gomez et al., "Skin laser treatments enhancing transdermal delivery of ALA," *J. Pharm. Sci.* **100**(1), 223–231 (2011).

20. S. L. Kilmer et al., "Treatment of epidermal pigmented lesions with the frequency-doubled Q-switched Nd:YAG laser," *Arch. Dermatol.* **130**(12), 1515–1519 (1994).
21. V. K. M. Poon, L. Huang, and A. Burd, "Biostimulation of dermal fibroblast by sublethal Q-switched Nd:YAG 532 nm laser: collagen remodeling and pigmentation," *J. Photochem. Photobiol. B-Biol.* **81**(1), 1–8 (2005).
22. H. L. Ee et al., "Treatment of acquired bilateral nevus of Ota-like macules (Hori's nevus) with a combination of the 532 nm Q-switched Nd:YAG laser followed by the 1,064 nm Q-switched Nd:YAG is more effective: prospective study," *Dermatol. Surg.* **32**(1), 34–40 (2006).
23. K. D. Polder et al., "Laser eradication of pigmented lesions: a review," *Dermatol. Surg.* **37**(5), 572–595 (2011).
24. V. V. Tuchin et al., "Light propagation in tissues with controlled optical properties," *J. Biomed. Opt.* **2**(4), 401–417 (1997).
25. C. G. Rylander et al., "Dehydration mechanism of optical clearing in tissue," *J. Biomed. Opt.* **11**(4), 041117 (2006).
26. Y. P. Kato et al., "Mechanical properties of collagen fibres: a comparison of reconstituted and rat tail tendon fibres," *Biomaterials* **10**(1), 38–42 (1989).
27. M. Wang, G. D. Pins, and F. H. Silver, "Collagen fibres with improved strength for the repair of soft tissue injuries," *Biomaterials* **15**(7), 507–512 (1994).
28. A. M. Kligman, "Perspectives and problems in cutaneous gerontology," *J. Invest. Dermatol.* **73**(1), 39–46 (1979).
29. A. E. Cerussi et al., "Spectroscopy enhances the information content of optical mammography," *J. Biomed. Opt.* **7**(1), 60–71 (2002).
30. M. Egawa et al., "Regional difference of water content in human skin studied by diffuse-reflectance near-infrared spectroscopy: consideration of measurement depth," *Appl. Spectrosc.* **60**(1), 24–28 (2006).
31. I. H. Blank, "Factors which influence the water content of the stratum corneum," *J. Invest. Dermatol.* **18**(6), 433–440 (1952).
32. R. M. Lavker et al., "Hairless micropig skin. A novel model for studies of cutaneous biology," *Am. J. Pathol.* **138**(3), 687–697 (1991).
33. N. J. Vardaxis et al., "Confocal laser scanning microscopy of porcine skin: implications for human wound healing studies," *J. Anat.* **190**(4), 601–611 (1997).
34. J. W. Pickering et al., "Double-integrating-sphere system for measuring the optical properties of tissue," *Appl. Opt.* **32**(4), 399–410 (1993).
35. S. A. Prahl, M. J. C. van Gemert, and A. J. Welch "Determining the optical properties of turbid media by using the adding-doubling method," *Appl. Opt.* **32**(4), 559–568 (1993).
36. T. Liu et al., "Characteristics of plasma plume expansion from Al target induced by oblique incidence of 1064 and 355 nm nanosecond Nd:YAG laser," *J. Phys. D: Appl. Phys.* **46**(48), 485207 (2013).
37. H. H. Pennes, "Analysis of tissue and arterial blood temperatures in the resting human forearm," *J. Appl. Physiol.* **85**(1), 5–34 (1998).
38. F. Xu et al., "Mathematical modeling of skin bioheat transfer," *Appl. Mech. Rev.* **62**(5), 050801 (2009).
39. L. V. Wang and H. I. Wu, *Biomedical Optics: Principles and Imaging*, John Wiley & Sons, Hoboken (2007).
40. A. Ishimaru, *Wave Propagation and Scattering in Random Media*, IEEE Press, Piscataway (1999).
41. V. Tuchin, *Tissue Optics: Light Scattering Methods and Instruments for Medical Diagnosis*, 2nd ed., SPIE Press, Bellingham (2007).
42. J. W. Pickering et al., "Changes in the optical properties (at 632.8 nm) of slowly heated myocardium," *Appl. Opt.* **32**(4), 367–371 (1993).
43. A. J. Welch and M. J. C. van Gemert, *Optical-Thermal Response of Laser-Irradiated Tissue*, Springer, Dordrecht (2011).
44. X. Ma et al., "Bulk optical parameters of porcine skin dermis at eight wavelengths from 325 to 1557 nm," *Opt. Lett.* **30**(4), 412–414 (2005).
45. H. Ding et al., "Determination of refractive indices of porcine skin tissues and intralipid at eight wavelengths between 325 and 1557 nm," *J. Opt. Soc. Am. A* **22**(6), 1151–1157 (2005).
46. M. Motamedi et al., "Light and temperature distribution in laser irradiated tissue: the influence of anisotropic scattering and refractive index," *Appl. Opt.* **28**(12), 2230–2237 (1989).
47. J. H. Yoo et al., "Explosive change in crater properties during high power nanosecond laser ablation of silicon," *J. Appl. Phys.* **88**(3), 1638–1649 (2000).
48. V. Venugopalan, N. S. Nishioka, and B. B. Mikic, "The thermodynamic response of soft biological tissues to pulsed ultraviolet laser irradiation," *Biophys. J.* **69**(4), 1259–1271 (1995).

Sungho Jeong is a professor at the Gwangju Institute of Science and Technology, Republic of Korea. He received a PhD degree in mechanical engineering from the University of California at Berkeley in 1997 and worked at the Lawrence Berkeley National Laboratory during his doctoral and postdoctoral studies. His research interests include laser ablation phenomena and their applications, and ongoing research includes application of laser-induced breakdown spectroscopy for thin film solar cell, laser shock peening, and laser interaction with biomedical materials.

Tae Joong Eom received his PhD degree in information and communications engineering from the Gwangju Institute of Science and Technology in 2005. He worked as a research scientist at Beckman Laser Institute of University California, Irvine, in 2008 and Washington University in Saint Louis in 2012. Since 2005, he has been a senior research scientist in the Advanced Photonics Research Institute. His research interests include biomedical imaging based on an optical coherence tomography and a photoacoustic microscopy.

Soogeun Kim is a PhD candidate at the Gwangju Institute of Science and Technology, Republic of Korea. He received a BS degree in mechanical engineering from Yeungnam University in 2004 and his MS degree in mechatronics from the Gwangju Institute of Science and Technology in 2007. His research interests include laser-tissue interaction mechanisms with low and high power laser and their applications, especially the effect of tissue conditions on laser-tissue interaction mechanisms.